J. Fluid Mech. (1973), *vol.* 59, *part* 4, *pp.* 791–801
Printed in Great Britain

The initial development of a submerged laminar round jet

By S. ABRAMOVICH AND A. SOLAN
Department of Mechanical Engineering, Technion, Haifa, Israel

(Received 21 February 1972 and in revised form 27 March 1973)

Experimental results are presented for the speed of travel of the spherical vortex at the front of a suddenly switched on, submerged, laminar jet in the Reynolds number range $80 < Re < 500$. The results show that the speed of advance of the front is approximately one half of the speed of a fluid element on the axis of the steady jet. The experimental data are well correlated by an approximate model of the jet–vortex interaction in which the vortex is treated as a liquid drop with averaged properties. An auxiliary result is a new correlation for the axial variation of the velocity of a steady jet.

1. Introduction

Instantaneous switching on of submerged laminar jets is widely used in fluid amplifiers of many types, and in turbulence amplifiers in particular. The knowledge of the transient behaviour of these jets is essential to the proper design of these amplifiers. Yet, though the steady-state behaviour of all types of jets has been studied quite extensively, it seems that relatively little is known regarding the initial transient process. Therefore, it is the purpose of the present paper to describe and analyse the transient behaviour of submerged jets in response to instantaneous switching on.

Visual information can be obtained by injecting dye into a liquid jet. One can then identify at the front of the suddenly operated jet a spherical ball of liquid, which increases in diameter and moves forward on the axis of the jet. (Photographs of such liquid balls have been published by Batchelor (1967); see in particular stages 1 to 6 in his figure 7.2.2, plate 20, taken from a paper by Okabe & Inoue.) Changes in the volume and velocity of the ball are due to some jet liquid entering the ball, carrying with it linear momentum and vorticity which are added to the momentum and vorticity of the liquid inside the ball. At the same time the forward motion of the ball is retarded by the fluid in the surroundings, which has to be accelerated in order to make way for the approaching jet. Because of the relative velocity between the ball and its surroundings, one must also take into account the momentum lost owing to viscous friction.

A detailed exact solution of this problem based on the full equations of motion including viscosity seems to be too complicated to be practical. Similarly, in view of the complicated geometry and the continuous axial movement, it is practically impossible to make direct measurements of the inner velocity field of

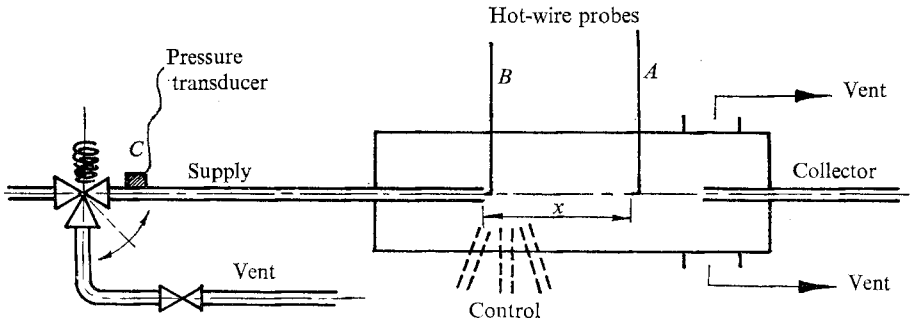

FIGURE 1. Experimental set-up.

the ball. Nevertheless, interesting and significant information can be obtained by measuring the forward axial motion of the ball as a whole, i.e. the distance of the ball from the tube exit as a function of time. This can be done with the aid of hot-film or hot-wire probes installed on the axis. Likewise, an approximate analytical solution can be obtained from a simplified model which regards the ball as a finite element and correlates its integral properties using overall conservation laws. This approach is similar to that of Turner (1957, 1959, 1962), who analysed the motion of droplets falling in a liquid under the action of gravity and of a rising buoyant plume.

In this paper we present the results of measurements of the forward motion of the ball, and an analytical solution based on a simplified integral model as described above. The experiments were made in the range Re = 80–500, which is of interest in turbulence amplifiers. The fluids used were water–glycerol mixtures and air. It will be seen that these results provide a reasonable physical picture of the phenomena and yield data directly relevant to the analysis of fluidic elements.

2. Experimental set-up

To investigate the transient behaviour of the jet for different values of viscosity, the measurements were carried out in air and in water–glycerol mixtures (68, 72 or 74 % glycerol). The apparatus used for the measurements in liquids was a large (20 × 20 × 80 cm) bath with a long tube protruding through the wall (figure 1). The tube's internal diameter was 12 or 6 mm and its length 1200 mm. For measurements in air the set-up was a 6 mm I.D. tube inside a 80 mm I.D. cylindrical wind tunnel.

The flow of liquid in the supply line was controlled by an electrically operated valve. A traversing hot-film probe was located on the tube axis. By repeating the switching process with the hot-film probe located at various distances x from the tube outlet, and measuring the time intervals between the valve opening and the appearance of a signal at the probe, a complete $x(t)$ record of the ball motion was obtained. Furthermore, after the ball has passed and the jet has become established, the same probe yielded a measurement of the steady-state velocity on the

jet axis. Each measurement was taken 3–5 times. The estimated overall experimental error is within $\pm 5\,\%$.

3. Steady-state jet

The maximum velocity in the established jet was measured in air and in water–glycerol mixtures in a range $Re = 80$–500 over axial distances $x/D = 0$–40, where $Re = U_0 D/\nu$ is the Reynolds number based on the tube diameter D and the mean tube velocity U_0. The results are best correlated in the form $U^* = U_{mx}/U_{m0}$ as function of $x^* = x/D\,Re^{\frac{1}{2}}$, where U_{mx} is the maximum velocity at x and U_{m0} is the maximum velocity at tube outlet. Assuming, as usual, that the maximum velocity of a given jet decreases in inverse proportion to the distance from a virtual source, we obtain the relation (figure 2)

$$U^* = 1/(ax^* + b), \quad a = 1{\cdot}13, \quad b = 0{\cdot}89, \tag{1}$$

which holds in the range $x^* > 0{\cdot}2$. This result can now be used to check whether momentum is conserved between the tube and the jet and to obtain an expression for the distance of the virtual source from the tube outlet. Recasting (1) in the familiar (dimensional) form

$$U_{mx} = A/\bar{x}, \tag{2}$$

where $\bar{x} = x + x_0$ is the distance from the virtual source and A is a constant for a given jet, we obtain from the present measurements, with $U_{m0} = 2U_0$ (parabolic profile in the tube),

$$A = U_{m0} D\,Re^{\frac{1}{2}}/a = 2\nu\,Re^{\frac{3}{2}}/a. \tag{3}$$

On the other hand, for the fully developed jet Schlichting (1968, p. 220) shows that

$$U_{mx} = \frac{3}{8\pi}\frac{M}{\rho\nu}\frac{1}{x}, \tag{4}$$

where M is the momentum. If one assumes that momentum is conserved in the developing region, then on equating the momentum of the jet with the momentum of the tube flow, $M/\rho = \frac{1}{8}\pi\,Re^2\nu^2$, one gets

$$A = \tfrac{1}{8}\nu\,Re^2, \tag{5}$$

which is in contradiction with our experimental result, equation (3). This shows that momentum is not conserved in the region of development, which has already been mentioned by Sato & Sakao (1964) for a two-dimensional jet, in which they found that the ratio of the jet momentum M to the pipe flow momentum M_0 is $M/M_0 = 0{\cdot}5$–$0{\cdot}8$, the loss being due to shear at the outer wall of the tube.

The distance x_0 of the virtual source from the tube outlet is obtained from (1) as

$$x_0 = (b/a)\,D\,Re^{\frac{1}{2}} = 0{\cdot}79 D\,Re^{\frac{1}{2}}, \tag{6}$$

which is at variance with Andrade & Tsien's (1937) often-quoted result

$$x_0 = 0{\cdot}04 D\,Re. \tag{7}$$

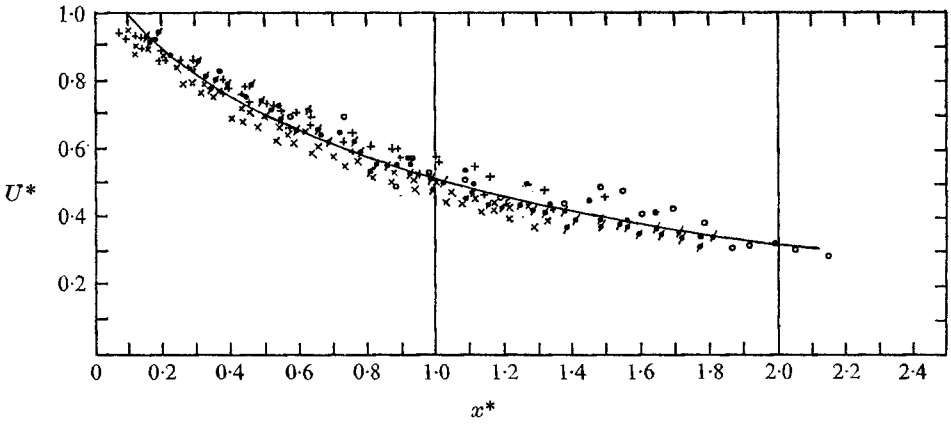

FIGURE 2. Maximum velocity of the jet. ●, air at 20 °C, 755 mm Hg; +, $D = 1{\cdot}2$ cm, $\nu = 0{\cdot}217$ cm²/s; ◐, $D = 0{\cdot}6$ cm, $\nu = 0{\cdot}148$ cm²/s; ×, $D = 1{\cdot}2$ cm, $\nu = 0{\cdot}148$ cm²/s; ○, Andrade & Tsien; ——, equation (1).

Figure 2 represents our experimental results for U_{mx}/U_{m0} versus $x^* = x/D\,Re^{\frac{1}{2}}$, including some points given by Andrade & Tsien, recalculated in terms of the present co-ordinates. By comparing our points with those of Andrade & Tsien, we find good agreement and, moreover, find that in the present scaling their experimental results are much better correlated than in the form (7) suggested by them originally. To see that the present form is more accurate, one should bear in mind the following points.

(i) Here we deal with a jet issuing from a long pipe, in order to have a fully developed parabolic profile at the outlet for every Reynolds number, while in Andrade & Tsien's work there is an uncertainty about this profile. (They assumed that for $Re > 80$ the profile at the exit of the tube was flat. Yet it is possible to show by recalculating their results that for some points $U_{mx}/U_0 > 1$, which means that the profile could not have been flat.)

(ii) Here we have results for different Reynolds numbers, different fluids and different pipe diameters, while Andrade & Tsien's results are based on experiments done for water and one pipe diameter only.

(iii) Andrade & Tsien's correlation is biased by the assumption that the momentum is conserved, which they used to calculate the velocity profiles of the jet based on the momentum in the pipe.

Thus our results (equation (1)), which are in good agreement with the generally accepted relation $U_{mx} = A/(x+x_0)$, show that the constants A and x_0 cannot be evaluated from an assumption of conserved momentum and from Andrade & Tsien's correlation but are given by the present equations (3) and (6).

4. Transient behaviour

4.1. *Experimental results*

The axial motion of the ball of fluid at the head of the jet yields the hot-film signals shown in figure 3. At each position x we can discern a time lag between

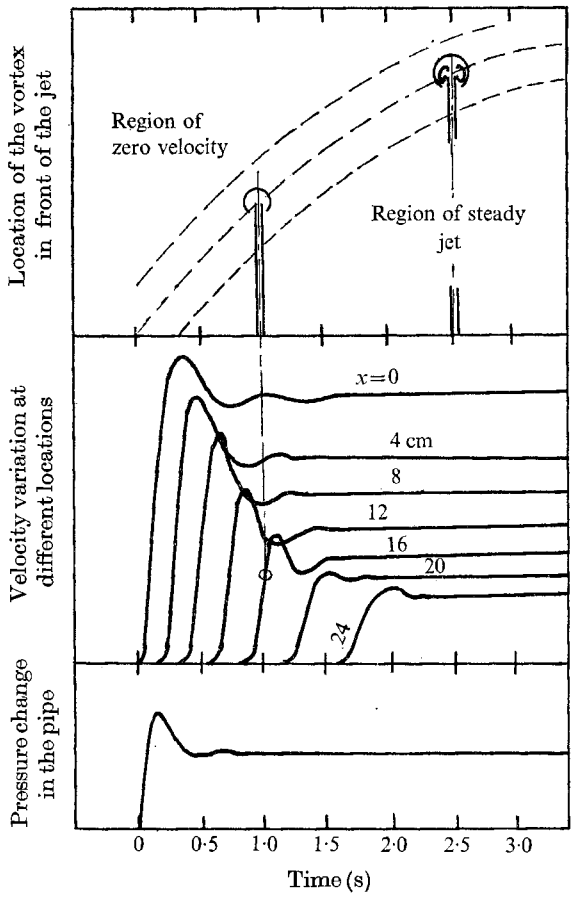

FIGURE 3. Velocity–time signals at different axial positions.

the moment when the ball leaves the tube outlet and the moment when a flow velocity is observed at x. Subsequently, there is a rise time, during which the velocity grows to its final steady value, corresponding to the steady (but not developed) jet. In some cases an initial overshoot was observed, and was probably due to internal circulation in the ball (recall that the axial velocity at the centre of Hill's spherical vortex is $\frac{3}{2}$ times the velocity of the vortex as a whole), but was also dependent on the rapidity of the valve opening. Since the transition between the rise period and the ultimate steady value (for which the jet is in the 'on' position) is smooth, we define the travel time t of the fluid ball as the time interval from the moment it leaves the tube outlet until the moment the velocity at x reaches 70 % of its final steady value. Clearly, this travel time t is a fundamental parameter in the analysis of fluidic elements.

Scaling x and U as before, and t accordingly, $t^* = 2t\nu Re^{\frac{1}{2}}/D^2$, we can plot t^* *vs.* x^* for various D, ν and U_0 (figure 4). Within the range of parameters dealt with here, the results are fairly well correlated by the relation

$$t^* = cx^{*2} + dx^*, \quad c = 1{\cdot}85, \quad d = 1{\cdot}6. \tag{8}$$

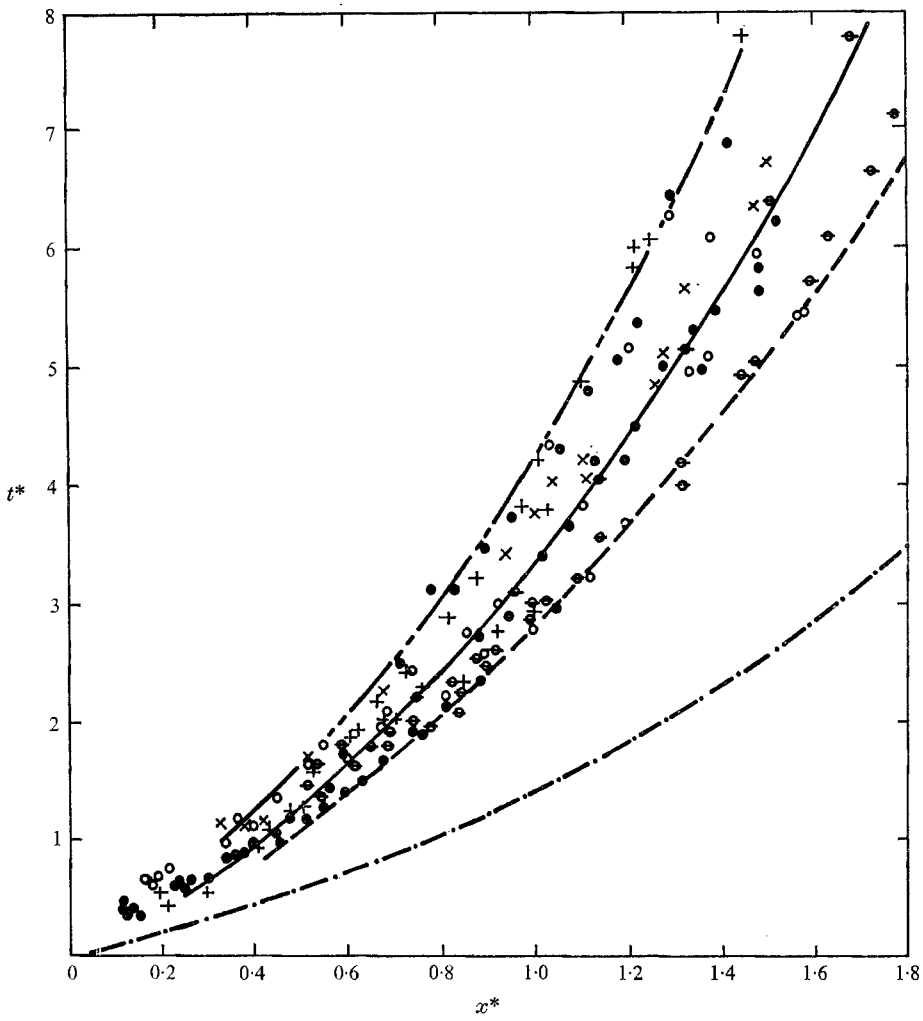

FIGURE 4. Travel time of ball as a function of distance: experimental. ×, air, $D = 0{\cdot}6$ cm. Glycerol: ●, $\nu = 0{\cdot}148$ cm²/s, $D = 1{\cdot}2$ cm; ○, $\nu = 0{\cdot}148$ cm²/s, $D = 0{\cdot}6$ cm; ⊖, $\nu = 0{\cdot}217$ cm²/s, $D = 1{\cdot}2$ cm; +, $\nu = 0{\cdot}256$ cm²/s, $D = 1{\cdot}2$ cm. ——, average travel time, equation (10); – –, minimum travel time; – · – ·, maximum travel time; – · –, travel time of a fluid element in steady jet, according to (1).

Hence we obtain the velocity of the ball:

$$U_B^* = dx^*/dt^* = 1/(2cx^* + d^*). \tag{9}$$

Note that, although the form of U_B^* in (9) is similar to that in (1), the numerical values of the coefficients are different, in accordance with the fact that the velocity of the ball is lower than the velocity of the fluid on the axis of the steady jet at the same axial position. The travel time of the ball is about twice as long as the travel time of a fluid element on the axis of the steady jet.

Examination of figure 4 shows that up to $x^* \approx 0{\cdot}7$ the points are distributed in a narrow band. For greater distances the points are much more scattered.

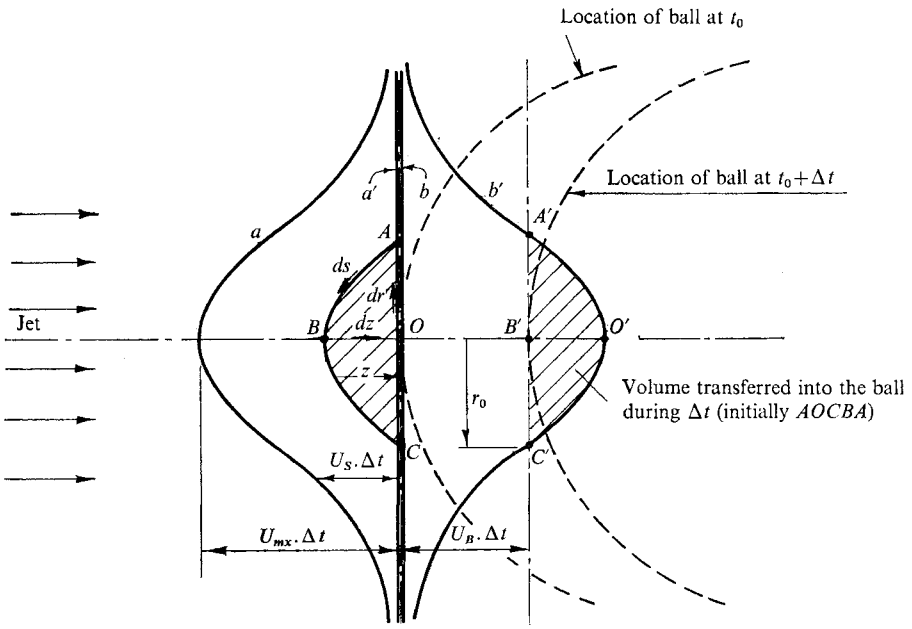

FIGURE 5. Interaction between jet and ball.

This fact can be explained as follows. For short distances the direction of the motion of the ball at the front of the jet is exactly axial. Later, because of instabilities (such as 'pedal breakdown'; see Reynolds 1962) the ball changes its direction. This change causes the increase in the time response, which cannot be defined exactly, but one can say that the line passing through the lowest points measured is that which describes the time response of a completely stable jet. This line can be represented in the same form as (10) except that the constants are changed, namely $c = 1{\cdot}4$ and $d = 1{\cdot}3$. On the other hand, for the design of fluidic elements one may need the maximum switching times, taking account of instabilities, given by the upper envelope in figure 4, which can be represented by (10) with $c = 2{\cdot}4$ and $d = 1{\cdot}95$.

4.2. *Theory: the liquid-drop model*

We consider the flow in the front of a suddenly operated jet as a spherical vortex flow interacting with a *steady* jet, and adopt an approximate model based on an integral momentum balance, similar to Turner's (1959) model.

A spherical mass with volume V_B travels on the axis of the jet with a velocity U_B (different from the maximum velocity U_{mx} of the jet at the same axial position). The jet impinges on the fluid ball, so that some fluid enters the ball and causes it to grow. In the absence of sufficient information on the details of the vortex flow we assume the following properties of the ball. The ball consists of fluid transferred from the jet only. Its velocity U_B is determined by the interaction between the ball and the jet and the drag forces between it and the surroundings as obtained from liquid-drop models (Winnikow & Chao 1966). No specific

assumption is made regarding the internal flow field in the ball. (In the present model we omit any possibilities of instabilities, which, in fact, are present.)

The interaction between the spherical mass and the jet is explained with the aid of figure 5. The jet is moving in the x direction. The tail of the vortex moving in the same direction is found at instant t at point O. If we draw on the jet two lines a and b at instant t_0 (the line a has a form similar to the velocity profile of the jet), at a later moment $t_0 + \Delta t$ the configuration of the lines will change so that we have lines a' and b' instead of a and b, while the ball located initially at O moves to B'.

The axial distance between a and a' is $U\Delta t$. Here we find that the quantity of fluid enclosed by the curve $OABCO$, which at t_0 is behind the vortex, is changed during Δt to that described by $O'A'B'C'O'$, which at time $t_0 + \Delta t$ is in front of point B' (the tail of the vortex). This means that this quantity has entered the vortex and become a part of it. This entrainment is characterized by the point A, which is the 'cut-off radius' or the position where the velocity of the jet and the velocity of the vortex are equal.

The entrained mass inflates the sphere and causes a change in its momentum. The influence of the fluid in front of the jet on the movement of the sphere can be separated into two parts.

(i) The liquid at some distance away from the ball is accelerated in nearly potential flow in order to make way for the approaching jet. This acceleration is associated with a rate of change of momentum (Milne-Thomson 1968, p. 491)

$$dM/dt = 0{\cdot}5\rho[d(U_B V_B)/dt]. \tag{10}$$

(ii) A thin film of liquid surrounding the ball has a viscous motion like a free boundary layer on a liquid sphere. The drag force on the sphere can then be represented as

$$F_D = C_D(\tfrac{1}{2}\rho U_B^2)(\tfrac{1}{4}\pi D_B^2), \tag{11}$$

where C_D is a drag coefficient. A reasonable approximation for this coefficient is to use data obtained for falling droplets, bearing in mind that the cases are not identical and that second-order effects will be different in the freely falling droplet and in the ball followed by a jet. In the present analysis the leading term of Winnikow & Chao's (1966) drag coefficient (for equal density and viscosity of the ball and surrounding fluid)

$$C_D = \frac{40}{Re_B}\left(1 + \frac{0{\cdot}814}{Re_B^{\frac{1}{2}}}\right) \tag{12}$$

was used and gave good agreement with experimental data. The leading term of Harper & Moore's (1968) improved theoretical expression $C_D = 120/Re_B$ was also tried, but gave results much higher than the measurements. Thus, apparently Winnikow & Chao's drag coefficient (12) is a good approximation for the drag on the ball pushed by a jet.

With these assumptions, the rate of change of the volume of the sphere due to the entrance of the jet is

$$\frac{dV_B}{dt} = 2\pi \int_0^{r_0} (U_S - U_B)\, r\, dr, \tag{13}$$

where $U_S(r)$ is the velocity of the jet, $U_S - U_B$ is its relative velocity and r_0 is the cut-off radius, at which the relative velocity is zero, and the rate of change of momentum is

$$\frac{dM_B}{dt} = \underbrace{\rho_0 \int_0^{r_0} (U_S - U_B)\, U_S\, 2\pi r\, dr}_{\substack{\text{Change of momentum due to} \\ \text{entrainment of the jet} \\ \text{into the ball}}} - \underbrace{\frac{\rho}{2}\frac{d(U_B V_B)}{dt}}_{\substack{\text{Acceleration} \\ \text{of virtual} \\ \text{mass}}} - \underbrace{F_D}_{\substack{\text{Drag} \\ \text{force}}}. \tag{14}$$

The two equations (13) and (14) determine the two unknown variables V_B and M_B (or D_B and U_B) as a function of time t, assuming that the velocity profile $U_S(r)$ is known.

Near the pipe exit ($x^* < 0{\cdot}2$) the jet profile can be assumed to be the same as in the pipe, i.e. parabolic:

$$U_S = U_{m0}[1 - (r/R_S)^2] \tag{15}$$

(at $x^* = 0{\cdot}2$ the difference between U_{m0} and U_{mx} is less than 10 %). In this region the cut-off radius is

$$r_0^2 = [1 - (U_B/U_{m0})]\, R_S^2. \tag{16}$$

The expression for the rate of change of volume of the spherical mass, equation (13), is then

$$dV_B/dt = Q_{S0}[1 - (U_B/U_{m0})]^2 \tag{17}$$

and the momentum equation (14) reduces, by straightforward manipulations, to

$$\frac{dU_B}{dt} = \frac{2}{3}\frac{M_0}{V_B}\left[1 - \frac{5}{4}\left(\frac{U_B}{U_{m0}}\right) + \frac{9}{2}\left(\frac{U_B}{U_{m0}}\right)^2 - \frac{7}{4}\left(\frac{U_B}{U_{m0}}\right)^3\right] - \frac{2}{3}\frac{F_D}{\rho V_B}, \tag{18}$$

where $M_0 = \frac{1}{3}R^2 U_{m0}^2$ is the kinematic momentum in the pipe. Introducing the dimensionless quantities x^*, t^* and U^* defined above, we find a set of three equations which have to be solved simultaneously:

$$\left.\begin{aligned} dV_B^*/dt^* &= (\pi/8Re_0)\,(1 - U_B^*)^2, \\ dU_B^*/dt^* &= (\pi/18Re_0\, V_B^*)\,(1 - \tfrac{5}{4}U_B^* + \tfrac{9}{2}U_B^{*2} - \tfrac{7}{4}U_B^{*3}) - \tfrac{1}{3}F^*, \\ dx^*/dt^* &= U_B^*. \end{aligned}\right\} \tag{19}$$

Here F^* is the non-dimensional form of $F_D/\rho V_B$:

$$F^* = \frac{F_D}{\rho V_B}\frac{DRe^{\frac{1}{2}}}{U_{m0}} = 0{\cdot}605\frac{U_B^{*2}}{V^{*\frac{1}{3}}}C_D. \tag{20}$$

These equations hold in the region in which the jet profile can be approximated by that of the pipe flow ($x^* \leqslant 0{\cdot}2$).

In the region $x^* > 0{\cdot}2$ we assume the interaction to be between a fully developed steady jet and a spherical ball. The jet velocity profile is

$$U_S = \frac{A}{\bar{x}}\frac{1}{[1 + B(r^2/\bar{x}^2)]^2}, \tag{21}$$

where $A/B = 8\nu$ and the flow rate is $Q_x = 8\pi\nu\bar{x}$. Here we get the cut-off radius as

$$r_0^2 = [(A/U_B\bar{x})^{\frac{1}{2}} - 1]\,\bar{x}^2/B. \tag{22}$$

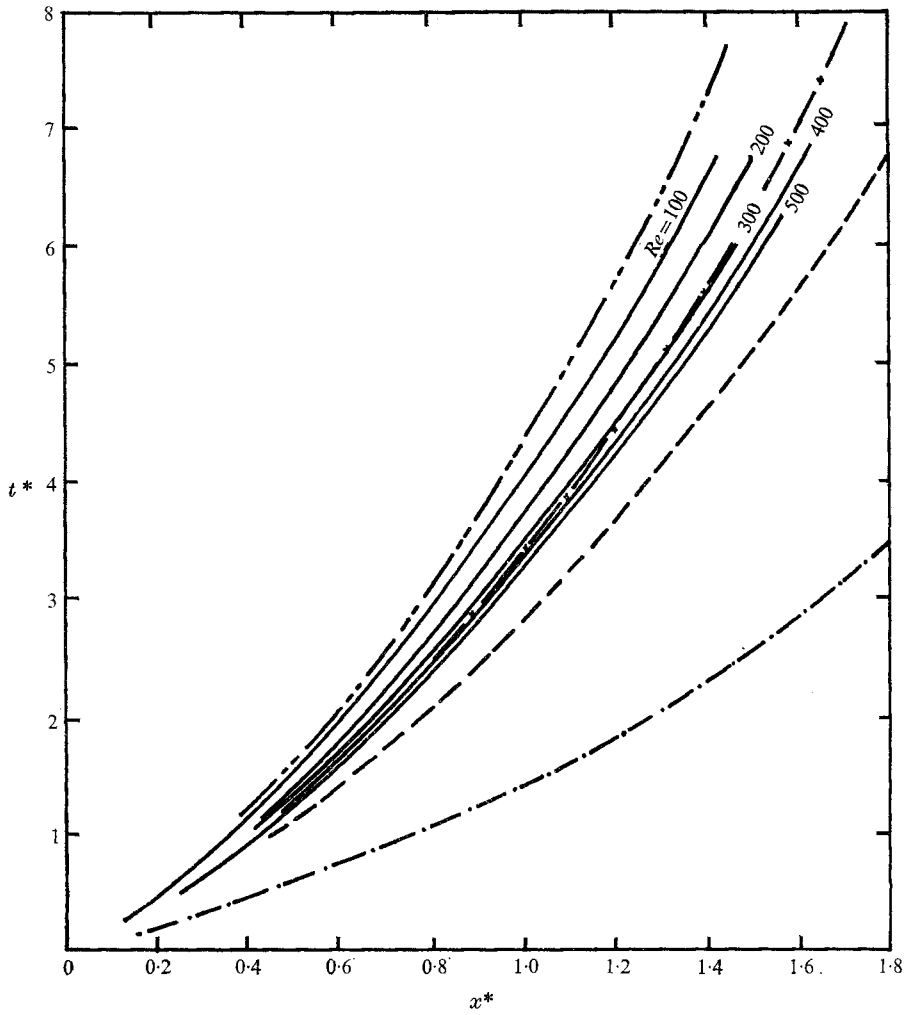

FIGURE 6. Travel time of ball as a function of distance. ——, theoretical. Experimental (70 % 'on'): –×–, average travel time; — —, minimum travel time; – – –, maximum travel time. –·–, travel time of a fluid element in steady jet, according to (1).

Substituting (22) and (21) into (13), we get the rate of change of volume of the spherical mass:

$$dV_B/dt = Q_x[1-(U_B/U_{mx})^{\frac{1}{2}}]^2, \tag{23}$$

where U_{mx} is the maximum velocity of the jet at point x. The momentum equation (14) yields, after some manipulation,

$$\frac{dU_B}{dt} = \frac{1}{1{\cdot}5V_B}\left\{8\pi\nu x_0 U_{m0}\left[\frac{1}{3}+\frac{11}{3}\left(\frac{U_B}{U_{mx}}\right)^{\frac{3}{2}}-\frac{5}{2}\frac{U_B}{U_{mx}}-\frac{3}{2}\left(\frac{U_B}{U_{mx}}\right)^2\right]-\frac{F_D}{\rho}\right\} \tag{24}$$

and, introducing again the non-dimensional variables, we obtain the set of equations for $x^* > 0{\cdot}2$:

$$\left.\begin{aligned} \frac{dV_B^*}{dt^*} &= \frac{4\pi}{Re_0^{\frac{3}{2}}} x^* \left[1 - \left(U_B^* \frac{x^*}{x_0^*}\right)^{\frac{1}{2}}\right]^2, \\ \frac{dU_B^*}{dt^*} &= \frac{4\pi}{1{\cdot}5} \frac{x_0^*}{V_B^*} \frac{1}{Re_0^{\frac{3}{2}}} \left[\frac{1}{3} + \frac{11}{3}\left(U_B^* \frac{x^*}{x_0^*}\right)^{\frac{3}{2}} - \frac{5}{2}\left(U_B^* \frac{x^*}{x_0^*}\right) - \frac{3}{2}\left(U_B^* \frac{x^*}{x_0^*}\right)^2\right] - \tfrac{2}{3}F^*, \\ dx^*/dt^* &= U_B^*. \end{aligned}\right\} \quad (25)$$

From flow visualization (cf., for example, Batchelor 1967) one can see that the initial shape of the vortex moving in front of the jet is that of a mushroom with a diameter approximately the same as the diameter of the pipe, the shape becoming spherical very soon afterwards. The diameter changes are small near the pipe outlet. Therefore, we take the initial value of the volume of the ball moving in front of the jet as that corresponding to the diameter of the pipe. Further, at the initial instant the ball is constrained by the pipe, so that the initial velocity of the ball is equal to the mean velocity in the pipe, which is assumed to undergo a nearly instantaneous step change.

The initial conditions for equations (19) are then

$$U_0 = U_{S\,\mathrm{mean}} = 0{\cdot}5 U_{S\,\mathrm{max}}, \quad V_0 = \tfrac{4}{3}\pi D^3. \quad (26)$$

The numerical results of (19) at $x^* = 0{\cdot}2$ are the initial conditions for (25).

Equations (19) and (25) were solved by a numerical procedure where we could easily change every parameter needed. (In fact, we could adopt different drag coefficients instead of (12) and also change the initial conditions.) The results are given in figure 6, which shows the distance versus time computed from the model, with drag forces defined by Winnikow & Chao, together with the experimental curves. It may be seen that the agreement is quite good, the computed results falling inside the band of scatter of the experimental data. Note that the theoretical model gives a weak dependence on the Reynolds number (in the x^*, t^* co-ordinates as defined here). In the experimental data, the dependence on *Re* is obscured by the scatter due to instabilities, which the present model cannot predict.

REFERENCES

Andrade, E. N. & Tsien, H. S. 1937 The velocity distribution in a liquid-into-liquid jet. *Proc. Phys. Soc.* **49**, 381.

Batchelor, G. K. 1967 *An Introduction to Fluid Dynamics*. Cambridge University Press.

Harper, J. F. & Moore, D. W. 1968 Motion of a drop at high Reynolds numbers. *J. Fluid Mech.* **32**, 367.

Milne-Thomson, L. M. 1968 *Theoretical Hydrodynamics*. Macmillan.

Reynolds, A. J. 1962 Observations of a liquid-into-liquid jet. *J. Fluid Mech.* **14**, 552.

Sato, H. & Sakao, F. 1964 An experimental investigation of the instability of a two-dimensional jet at low Reynolds numbers. *J. Fluid Mech.* **20**, 337.

Schlichting, H. 1968 *Boundary Layer Theory*. McGraw-Hill.

Turner, J. S. 1957 Buoyant vortex rings. *Proc. Roy. Soc.* A **239**, 61.

Turner, J. S. 1959 A comparison between buoyant vortex rings and vortex pairs. *J. Fluid Mech.* **7**, 419.

Turner, J. S. 1962 The 'starting plume' in neutral surroundings. *J. Fluid Mech.* **13**, 356.

Winnikow, S. & Chao, B. T. 1966 Droplet motion in purified systems. *Phys. Fluids*, **9**, 50.